














Bridging the Terahertz Gap: Photonics-Assisted Free-Space Communications From the Submillimeter-Wave to the Mid-Infrared

Xiaodan Pang , Senior Member, IEEE, Oskars Ozolins , Member, IEEE, Shi Jia , Lu Zhang , Richard Schatz , Aleksejs Udalcovs , Senior Member, IEEE, Vjaceslavs Bobrovs , Hao Hu , Toshio Morioka , Yan-Ting Sun , Jiajia Chen , Sebastian Lourduoss, Senior Member, IEEE, Leif Katsuo Oxenløwe, Sergei Popov , and Xianbin Yu , Senior Member, IEEE

(Invited Paper)

Abstract—Since about one and half centuries ago, at the dawn of modern communications, the radio and the optics have been two separate electromagnetic spectrum regions to carry data. Differentiated by their generation/detection methods and propagation

Manuscript received November 15, 2021; revised January 24, 2022; accepted February 18, 2022. Date of publication February 23, 2022; date of current version May 25, 2022. This work was supported in part by the Swedish Research Council (VR) under Grants 2019-05197 and 2016-04510, in part by the EU H2020 Project cFLOW under Grant 828893, in part by the by COST Action under Grant CA19111 NEWFOCUS, in part by the ERDF-funded CARAT Project under Grant 1.1.1.2/VIAA/4/20/660, in part by the Independent Research Fund Denmark under Grant 9041-00395B, in part by the National Key Research and Development Program of China under Grant 2020YFB1805700, in part by the National Natural Science Foundation of China under Grants 62101483 and 61771424, in part by the Natural Science Foundation of Zhejiang Province under Grants LQ21F010015 and LZ18F010001, and in part by Zhejiang Lab under Grant 2020LCOAD01. (Corresponding authors: Xiaodan Pang; Shi Jia; Xianbin Yu.)

Xiaodan Pang is with the Applied Physics Department, KTH Royal Institute of Technology, 10691 Stockholm, Sweden, and also with the Networks Unit, RISE Research Institutes of Sweden, 16440 Kista, Sweden (e-mail: xiaodan@kth.se).

Oskars Ozolins is with the Applied Physics Department, KTH Royal Institute of Technology, 10691 Stockholm, Sweden, with the Applied Physics Department, KTH Royal Institute of Technology, 10691 Stockholm, Sweden, and also with the Institute of Telecommunications, Riga Technical University, 1048 Riga, Latvia (e-mail: oskars.ozolins@ri.se).

Shi Jia, Hao Hu, Toshio Morioka, and Leif Katsuo Oxenløwe are with the DTU Fotonik, Department of Photonics Engineering, Technical University of Denmark, DK-2800 Kgs. Lyngby, Denmark (e-mail: shijai@fotonik.dtu.dk; huhao@fotonik.dtu.dk; tomo@fotonik.dtu.dk; lkox@fotonik.dtu.dk).

Richard Schatz, Yan-Ting Sun, Sebastian Lourduoss, and Sergei Popov are with the Applied Physics Department, KTH Royal Institute of Technology, 10691 Stockholm, Sweden (e-mail: rschatz@kth.se; yasun@kth.se; slo@kth.se; sergeip@kth.se).

Lu Zhang and Aleksejs Udalcovs are with the Networks Unit, RISE Research Institutes of Sweden, 16440 Kista, Sweden DTU Fotonik, Department of Photonics Engineering, Technical University of Denmark, DK-2800 Kgs. Lyngby, Denmark (e-mail: zhanglu1993@zju.edu.cn).

Xianbin Yu is with the College of Information Science and Electronic Engineering, Zhejiang University, Hangzhou 310027, China, and also with the Zhejiang Lab, Hangzhou 310000, China (e-mail: xyu@zju.edu.cn).

Vjaceslavs Bobrovs is with the Institute of Telecommunications, Riga Technical University, 1048 Riga, Latvia (e-mail: vjaceslavs.bobrovs@rtu.lv).

Jiajia Chen is with the Electrical Engineering Department, Chalmers University of Technology, SE-412 96 Gothenburg, Sweden (e-mail: jjajiac@chalmers.se).

Color versions of one or more figures in this article are available at <https://doi.org/10.1109/JLT.2022.3153139>.

Digital Object Identifier 10.1109/JLT.2022.3153139

properties, the two paths have evolved almost independently until today. The optical technologies dominate the long-distance and high-speed terrestrial wireline communications through fiber-optic telecom systems, whereas the radio technologies have mainly dominated the short- to medium-range wireless scenarios. Now, these two separate counterparts are both facing a sign of saturation in their respective roadmap horizons, particularly in the segment of free-space communications. The optical technologies are extending into the mid-wave and long-wave infrared (MWIR and LWIR) regimes to achieve better propagation performance through the dynamic atmospheric channels. Radio technologies strive for higher frequencies like the millimeter-wave (MMW) and sub-terahertz (sub-THz) to gain broader bandwidth. The boundary between the two is becoming blurred and intercrossed. During the past few years, we witnessed technological breakthroughs in free-space transmission supporting very high data rates, many achieved with the assistance of photonics. This paper focuses on such photonics-assisted free-space communication technologies in both the lower and upper sides of the THz gap and provides a detailed review of recent research and development activities on some of the key enabling technologies. Our recent experimental demonstrations of high-speed free-space transmissions in both frequency regions are also presented as examples to show the system requirements for device characteristics and digital signal processing (DSP) performance.

Index Terms—Free-space communication, quantum cascade laser, terahertz communication, terahertz photonics.

I. INTRODUCTION

THE ongoing digital transformation of our society relies on fast and secure ICT infrastructure. Many prominent aspects of large-scale digitalization, such as the Internet of Things (IoT), autonomous vehicles, augmented reality (AR), and tactile internet, have already started and will continue to reshape our society. Since about four decades ago, orders of magnitudes of higher bandwidth demand have been gradually supported by the evolution of mobile communications from the second generation (2G) to the fifth generation (5G), which is under deployment today. Accordingly, the adopted wireless carrier frequencies have been pushed to increase step by step from the microwave to the millimeter-wave (MMW) [1]. Recent market analysis reports that the year-on-year growth of the global mobile data

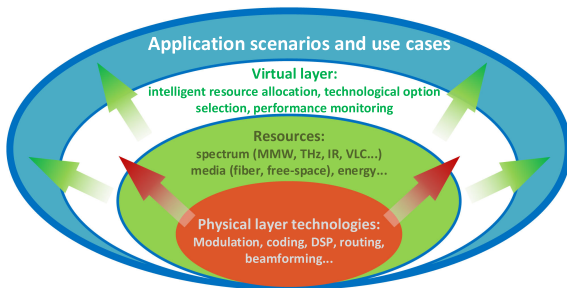


Fig. 1. A vision of an all-spectra communication paradigm to create a sustainable technological roadmap beyond next generations of wireless/wireline networks to unlock future bandwidth limit.

traffic is around 50% in the first and second quarters of 2021, and the total traffic is projected to increase almost five-fold in the upcoming four-year time span. Simultaneously, short-range Internet of Things (IoT) connections are expected to grow almost four-fold [2]. For many of these emerging time-critical applications, instantaneous transfer of large-volume uncompressed data between the end units and the edge aggregation is essential [3]. In this context, radio technologies face a sign of saturation in their roadmap horizon to support future mobile services. Current radio technologies have difficulties providing equivalent support for emerging time-critical applications since traditional microwave solutions are reaching their physical upper limit on available bandwidth. Through advances in the physical layer (PHY) design, such as massive multiple-input multiple-output (m-MIMO) techniques, improvements in spectral efficiency are possible [4]. The use of the MMW bands may also alleviate the spectrum crunch problem for wireless access in the short term. Nevertheless, regardless of such potential gains in spectral efficiency and resource, much broader bandwidths will be required to cope with the predicted data traffic growth.

A necessary paradigm shift in wireless communications is envisioned for beyond-5G (B5G) or 6G era. As the continuously increased wireless carrier frequency enters the terahertz (THz) scale, the boundary between the radio and optics becomes blurred and inter-crossed. Therefore, it is natural to consider the optical spectrum, where abundant spectral resources are available compared with the RF, as a part of the next-generation wireless communication infrastructure to deliver information jointly [5]. Fig. 1 presents a vision of such an all-spectra communication paradigm for future B5G/6G communication. In this vision, a unified ultrabroad electromagnetic (EM) spectral resource pool composing both optics and RF spectrum bands is available to be allocated for wireless services. Though heterogeneous in propagation properties and corresponding physical layer technologies, different spectrum regions can be collectively controlled from a virtual layer, which performs capacity analysis, resource allocation, performance monitoring and prediction, system optimization. In such a way, the actual physical technologies can become transparent to the bandwidth-intensive applications in the end premises. Eventually, we can realize ‘instant bandwidth’ availability per demand.

The standard definition of RF contains (but is not limited to) microwave, MMW, and sub-MMW (sub-THz), and the traditional definition of optics includes ultraviolet, visible light (VL),

and infrared (IR). More elaborately, the IR region can be decomposed into short-wave infrared (SWIR), mid-wave infrared (MWIR), and long-wave infrared (LWIR). The maturity levels of research and development in these regions vary considerably. On the one hand, though limited in bandwidth, the microwave has been intensively developed and deployed for decades for wireless communications. The MMW and the VL are currently being developed and may be deployed in the short term. The SWIR (1.55 μm band), also referred to as the telecom band, has also been available in commercial free-space communication systems. It is mainly because of the maturity of active and passive components and devices driven by fiber-optics. However, a significant drawback is its very high sensitivity to atmospheric channel perturbations such as dust, fogs, and turbulence effects such as scintillation, beam broadening and beam wandering, which can be effectively reduced or even eliminated by moving to a longer wavelength. Subsequently, the two atmospheric transmission windows at the MWIR (3-5 μm) and the LWIR (9-12 μm) become attractive for mid- and long-range outdoor applications, owing to their merits of low propagation attenuation ($< 1\text{dB/km}$) and robustness against weather conditions [6]. On the other hand, the sub-MMW, or referred to as the lower-THz band, and the MWIR/LWIR, referred to as the upper-THz band, are only in the early stages of research and have much lower technology readiness levels (TRLs) compared with other regimes in the scope of communications. Nevertheless, there are enormous potentials buried in these bands, and photonic technologies can be the key to leveraging them.

In this paper, we extend our ECOC contribution [7] and provide a more detailed review and outlook on different aspects of current free-space communication technologies in the THz region. Notably, we focus on the role of photonic technologies and elaborate their operational principles of supporting high-speed transmissions in both the sub-MMW and the MWIR/LWIR region. The rest of this paper is organized as follows: in Section II, we present a summary of state of the art in free-space transmission demonstrations in both the lower- and upper-THz bands enabled by various approaches. Section III describes the detailed operational principles and methodologies that we have adopted in our experimental studies. Section IV shows a few examples of our recent experimental demonstrations in high-speed free-space transmissions in both the lower- and upper-THz bands and discusses the system performance limits. Finally, we give our conclusions and outlook in Section V.

II. STATE OF THE ART

In recent years, we have witnessed tremendous research and development efforts in THz communications with different approaches. In the lower-THz band, there are many system-level demonstrations either with an all-electronic approach or with a photonics-assisted approach. In the upper-THz band, all-optical schemes dominate the system-level studies, as it is more straightforward to translate optical technologies from the SWIR telecom band to this region. This section summarizes the state-of-the-art free-space transmission works in both frequency regions and reviews the key enabling technologies to provide an overall picture of the research frontline.

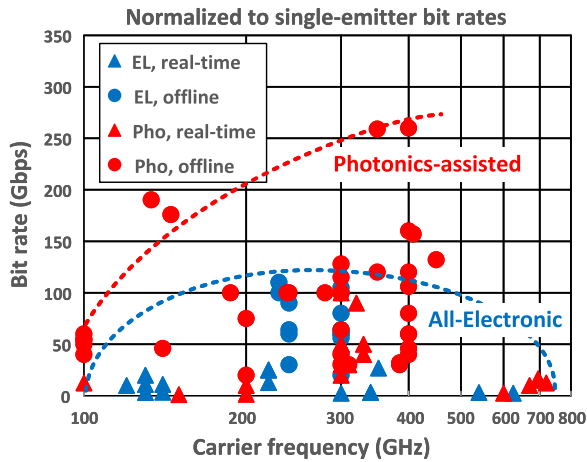


Fig. 2. A non-exhaustive summary of the state of the art in transmission demonstrations in the lower-THz band [8]–[69]. All system transmission speeds are normalized to single-emitter net bit rates. Blue markers represent all-electronic schemes and red markers are photonics-assisted schemes. Triangle markers represent real-time transmission demonstrations, whereas round markers are demonstrations performed with offline signal processing.

A. Lower-THz Band: High-Speed Sub-MMW Transmissions

Fig. 2 shows a non-exhaustive summary of the state-of-the-art lower-THz transmission demonstrations, including both the all-electronic and photonics-assisted systems. In what follows, we elaborate on each approach.

1) *All-Electronic Approach*: The electromagnetic waves in the lower-THz band mainly fall into the categories of MMW (< 300 GHz) and sub-MMW (> 300 GHz) regimes. Therefore, they have closer propagation properties as the radio waves rather than the optical waves. In terms of wireless data transmissions in this frequency range, all-electronic approaches are the most straightforward path to follow, owing to the accumulated expertise and momentum of the microwave technologies from the past and current generations of wireless systems.

There have been many high-speed data transmission demonstrations using III-V and silicon technologies for carrier frequencies up to 300 GHz (MMW range), particularly below 200 GHz. Demonstrations of 10 Gb/s real-time transmissions over a 1-km distance were achieved in the 120 GHz band [8], [9]. For systems with carrier frequencies of above 200 GHz, millimeter-wave monolithic integrated circuits (MMICs) with InP and InGaAsP-based high-electron-mobility transistors (HEMT) and metamorphic HEMT (mHEMT) are developed and employed to generate and receive over 10 Gb/s or even 100 Gb/s signals [10]–[16]. Recently, up to 100 Gb/s transmissions are also demonstrated with Si-based CMOS [17]–[19] and SiGe-based BiCMOS heterojunction bipolar transistors (HBT) technologies [20], [21] at 240 GHz or 300 GHz. Transceiver technologies based on these all-electronic schemes are expected to be compact and energy-efficient.

Generation and detection of high-bandwidth signals above 300 GHz, i.e., sub-MMW frequencies, impose higher engineering challenges during RF integration and packaging. As one can observe from the saturating tendency shown in Fig. 2, achieving broad bandwidth and high power simultaneously in the sub-MMW region is yet to be seen. There are recently a few

demonstrations reported with resonant tunnel diodes (RTD)-based oscillators and coherent receivers operating at around 350 GHz [22]–[24]. Up to 25 Gb/s real-time transmissions are achieved with RTDs at both the transmitter and the receiver [24]. One should note that the summarized tendency (shown as the blue curve in Fig. 2) only reflects the current research status reported in the literature rather than a forecast of the future research and development trend. More high-bitrate demonstrations are expected to be carried out in the near term considering the increasing research efforts devoted to this area.

To summarize, all-electronic approaches, particularly the Si technologies, are expected to be developed and deployed in large volumes to support use cases up to 300 GHz. The bandwidth and the corresponding data rate scalability of these all-electronic schemes remain to be seen at higher frequencies.

2) *Photonics-Assisted Approach*: The optical and photonic technologies have been proven successful in wireline systems. Since several decades ago, they have first conquered the telecom networks worldwide with the fast replacements of coaxial cables by optical fibers. Recently, high-speed optical interconnect technologies are also being widely deployed in datacom networks. The main intrinsic advantage of photonic technologies is the ultrabroad bandwidth in the optical frequencies. Broadband optoelectronic devices have facilitated high-speed data modulation and reception at the order of terabit-per-second (Tb/s) in the digital coherent optical systems. The recent research activities in microwave photonics have established a bridge to directly utilize the broadband characteristics of the photonics technologies in RF applications, including high-speed communications [25]–[28]. MMW and THz radio-over-fiber and photonic-wireless transmissions have been intensively studied and demonstrated in the past decade [29]. Many photonics-assisted high-speed transmission system demonstrations have been reported in the W-band (75–110 GHz) and the D-band (110–170 GHz) [30]–[38]. Most of these MMW photonic-wireless transmissions are based on high-speed p-i-n photodiodes (PDs).

In recent years, with the maturity and even commercial availability of fast-response uni-traveling carrier photodiode (UTC-PD) [40], [41], an increasing number of transmission demonstrations with advanced modulation formats are performed in higher frequency bands, e.g., above 200 GHz [42]–[48]. A 100 Gb/s multicarrier signal transmission was reported in the 200 GHz band with a gain-switched laser comb source [42]. Koenig *et al.* reported a record single-channel 100 Gb/s transmission at 237.5 GHz over 20-m distance with UTC-PD-based transmitter and InGaAsP mHEMT MMIC receiver [43]. A self-coherent THz link of 115 Gb/s net rate over 110-m distance was demonstrated at 300 GHz based on the Kramers-Kronig approach [49]. We have carried out several system-level studies with single-channel and multidimensional-multiplexed system configurations at the 350 GHz – 400 GHz region [50]–[61]. A few selected examples are elaborated on in Section IV. Most of these works are based on offline digital signal processing (DSP) and benchmark the BER performances against the pre-forward-error-correction code (pre-FEC) threshold. This method is considered a common practice in digital coherent optical systems in fiber-optic communications. Lately, a real-time fiber-wireless link at 300 GHz with a gross data rate of 136 Gb/s was reported

using a digital coherent modem [62]. Nevertheless, the use of DSP and advanced FEC inevitably introduces latency, which becomes less favorable for specific high-end time-sensitive applications [63]. Accordingly, tremendous research efforts have also been devoted to achieving real-time “error-free” transmissions with BER below 1×10^{-9} without the use of DSP [64]–[69]. With the assist of photonic processing techniques in the analog domain, up to 100 Gb/s real-time QPSK signal was successfully transmitted at 300 GHz [65], and up to 15 Gb/s transmission was demonstrated at the >600 GHz band [69].

B. Upper-THz Band: Mid-Wave and Long-Wave Infrared

The upper-THz band can be loosely categorized as the frequency bands above 1 THz up to tens of THz, overlapping with the MWIR and the LWIR. Compared with the lower-THz region, which is recognized by the wireless communication community as the “Next Frontier” [70], research activities on free-space communications in the MWIR/LWIR based are much fewer. There are mainly two photonic approaches in generating and detecting signals, i.e., wavelength conversion and directly emitting laser sources.

1) *Wavelength Conversion Approach*: Whenever possible, it is easier and preferable to reuse the mature optical and optoelectronic components and devices from the fiber-optic systems for free-space transmissions. Therefore, wavelength conversion from the telecom band has been proposed and is often used for free-space transmissions in the MWIR range. Nonlinear parametric conversions in periodically poled LiNbO₃ (PPLN) devices pumped by a high-power laser around 1- μm are often used for wavelength conversion between the telecom band and the MWIR [71]. In such a scheme, the wavelength is up-converted and down-converted to/from MWIR before and after the free-space link [72]–[75]. Therefore, both the transmitter and receiver can directly operate in the telecom band, e.g., 1.55 μm . Subsequently, with such an approach, the data rates of the MWIR free-space link can keep up with the development of fiber-optic systems. One of the first demonstrations with such a scheme was reported by Ip *et al.* with a real-time 2.488 Gb/s QPSK transmission at 3.8 μm [72]. Recently, single-channel transmissions at 3.5 μm with up to 10 Gb/s data rate are demonstrated with both DPSK [76] and QPSK signal formats [77]. Zou *et al.* further extended this approach into a multi-dimensional multiplexing system and demonstrated a 300 Gb/s aggregated data rate at 3.4 μm [78].

There are several advantages of such a wavelength-conversion approach. It can support very high data rates and is seamlessly compatible with fiber-optic systems. Moreover, it can be quickly installed for high-end applications. However, there are also certain drawbacks. Firstly, most of the demonstrated transmissions, if not all, are limited to below 4 μm region. Therefore, it can be challenging to cover the two optimal atmospheric transmission windows around 4.5 μm and 9 μm with such a scheme [6]. Secondly, the parametric frequency conversion process requires high pump power, resulting in relatively low energy efficiency. Finally, the PPLN devices are often bulky, making such a scheme challenging to miniaturize for large-volume deployable transceivers.

2) *Direct Emission Sources*: From the energy efficiency point of view, direct emission laser sources at the MWIR and LWIR regions are favorable because of easy integration and exemption from frequency conversion-induced power loss. One of the earliest explorations of using a direct emitting MWIR source was reported in [79], where a PbCdS diode laser at 3.5 μm was used to transmit 100 Mb/s data. The speed of this work was limited by carrier lifetime. In the 90s, the invention of the quantum cascade laser (QCL) opened opportunities for developing compact semiconductor transceivers for free-space communications [80]. Unlike the semiconductor lasers based on inter-band transitions, QCLs exploit inter-subband transitions and cover a wide wavelength range over the MWIR and LWIR. Later improvements in their distributed-feedback structure design [81] and continuous-wave (CW) operation [82] further enhanced the viability of QCLs for a wide range of applications, free-space communications included. More importantly, QCLs have very high intrinsic modulation bandwidth, owing to their extremely short carrier relaxation lifetime [83]. A few free-space transmission demonstrations based on directly modulated (DM) QCLs with a data rate of up to a few Gb/s have already been reported since the early 2000s [84]–[90]. Since 2007, with the invention of THz QCLs [91], several transmission experiments have been reported with up to tens of Mb/s data rate [92]–[95]. Nevertheless, most of these demonstrations in the early years required the QCLs to be operated at cryogenic temperatures. A few years later, room-temperature broadband modulation of QCLs was made possible in the MWIR and LWIR regions [96], [97]. Consequently, a few QCL-based free-space transmission demonstrations at room-temperature have been reported since then [98]–[105]. A non-exhaustive summary of QCL-based free-space transmission experiments is presented in Table I. Key specifications, including the operational wavelength, the transmitted signal data rate or bandwidth, the employed modulation format, the free-space channel, and the operational temperature, are listed. Our recent experimental studies employing advanced modulation formats and DSP are also included in Table I [102]–[106]. We further elaborate on the implementation details of these works in Section IV. It is worth noting that MWIR/LWIR free-space transmissions based on external modulation has also emerged as a promising research direction. A very recent experimental demonstration of up to 10 Gb/s NRZ transmission at 9 μm was reported, showing promising transceiver properties to further support multilevel modulation formats [107].

III. METHODS AND OPERATION PRINCIPLES

This section describes the commonly used methods and operation principles for signal generation, detection, and processing in photonics-assisted transmission systems for lower- and the upper-THz bands.

A. Hybrid Electro-Optical Systems in the Lower-THz Band

Fig. 3 illustrates a generic system configuration for hybrid electro-optical THz transmissions, including the broadband THz signal generation based on heterodyne photomixing and the coherent down-conversion based on heterodyne receiver.

TABLE I
SUMMARY OF EXPERIMENTAL DEMONSTRATIONS OF DM QCL-BASED FREE-SPACE TRANSMISSIONS WITH >1 THZ CARRIER FREQUENCIES

Wavelength	Data rate/ bandwidth ^a	Modulation format	Channel	QCL operation temperature	Reference
7.3 μm	10 MHz ^b	Analog signal	70 m indoor	80 K	[84]
8.1 μm	2.5 Gb/s	NRZ	1 m	85 K	[85],[86]
8.1 μm	750 MHz-1.5 GHz	Multi-channel QPSK	100 m outdoor	25 K	[87]
9.3 μm	330 MHz / 115 kb/s	Analog / NRZ ^c	350 m outdoor/10 m indoor	288 K	[88]
10.46 μm	20 kHz	Pulse frequency modulation	6000 m outdoor	240 K-340 K	[89]
3 μm	70 Mb/s	NRZ	1 m	77 K	[90]
73 μm	580 kHz	Analog signal	2 m	10 K	[92]
72.6 μm	1 Mb/s	NRZ	2.2 m	13 K	[93]
77 μm	5 Mb/s	NRZ	2.4 m	10 K	[94]
92 μm	20 Mb/s	NRZ	2.2 m	11 K	[95]
4.7 μm	40 MHz	Analog video signal	2.5 m	Room-temperature ^c	[98]
Mid-IR ^d	20 MHz	32-ary PPM	Turbulence simulator	Un-cooled ^e	[99]
10.6 μm	1 Gb/s	NRZ	Not specified	298 K	[100]
4 μm	680 Mb/s	RZ	1 m	288 K	[101]
4.65 μm	3 Gb/s	NRZ, PAM-4, PAM-8	5 cm	293 K	[102]
4.65 μm	4 Gb/s	PAM-4, DMT	5 cm	293 K	[103],[104]
4.65 μm	6 Gb/s	PAM-8	50 cm	293 K	[105],[106]

^aThe data rate for digital transmission, and modulation bandwidth for analog transmission are listed, respectively; ^b modulated on to a 66 MHz carrier; ^c operation temperature not explicitly specified; ^d wavelength not explicitly specified.

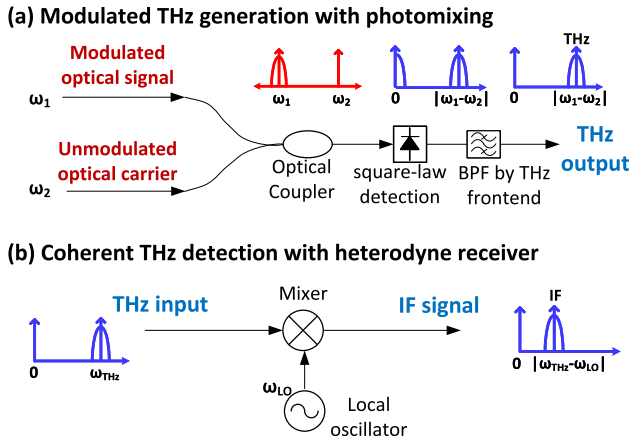


Fig. 3. Principles of (a) photomixing-based THz generation, which “transparently” converts the phase and amplitude modulation from optical carrier to THz carrier and (b) the coherent THz detection with electrical heterodyne receiver.

1) *Generation of Broadband Modulated THz Signal:* Fig. 3(a) presents the principle of broadband modulated THz signal generation based on optical heterodyne photomixing. In this example, two continuous optical waves with angular frequencies of ω_1 and ω_2 ($\omega_1 \neq \omega_2$) can be generated in the near-IR telecom band (e.g., 1.55 μm) with semiconductor lasers, and one of the optical waves is modulated with complex signals in both amplitude and phase at a fiber-optic IQ modulator. The other optical wave can remain unmodulated and serve as a carrier. These two signals can be expressed as:

$$E_1(t) = A_1(I + jQ)e^{-j(\omega_1 t + \varphi_1)} \quad (1)$$

$$E_2(t) = A_2 e^{-j(\omega_2 t + \varphi_2)} \quad (2)$$

where I and Q represent the two modulated orthogonal components in the complex plane, i.e., the in-phase and the quadrature signals. A_1 and φ_1 are the optical field amplitude and phase of the signal wave. Similarly, A_2 and φ_2 are the amplitude and phase of the carrier wave. The two optical waves are combined and launched into a fast response photomixer, such as the UTC-PD, for a square-law detection. Assuming the conversion efficiency of the photomixer is η_{Tx} , the square-law process can be expressed as:

$$E_{output} = \eta_{Tx} \cdot [E_1(t) + jE_2(t)]^2 = E_{baseband}(t) + E_{THz}(t) \quad (3)$$

One should note that noise is not included in the derivations for simplicity purposes. As shown in (3), after the square-law detection, the output signal from the photomixer consists of a baseband component generated from self-beatings from both the carrier and the signal, and a radiofrequency (RF) component in the THz and centered at a frequency of $\omega_{THz} = |\omega_1 - \omega_2|$. In most THz emitters, the baseband component is usually bandpass filtered out by the waveguide and the antenna, leaving only the THz component expressed as:

$$E_{THz}(t) = A_{THz} [I \cdot \sin(\omega_{THz} t + \varphi_{THz}) + Q \cdot \cos(\omega_{THz} t + \varphi_{THz})] \quad (4)$$

with $A_{THz} = 2\eta_{Tx} A_1 A_2$ and $\varphi_{THz} = \varphi_1 - \varphi_2$ the amplitude and the phase of the generated THz wave, respectively. From (4), one can see that although such a heterodyne photomixing is a nonlinear process, the modulated signal amplitudes and the orthogonality of the in-phase and quadrature components are linearly preserved. In other words, the modulated information

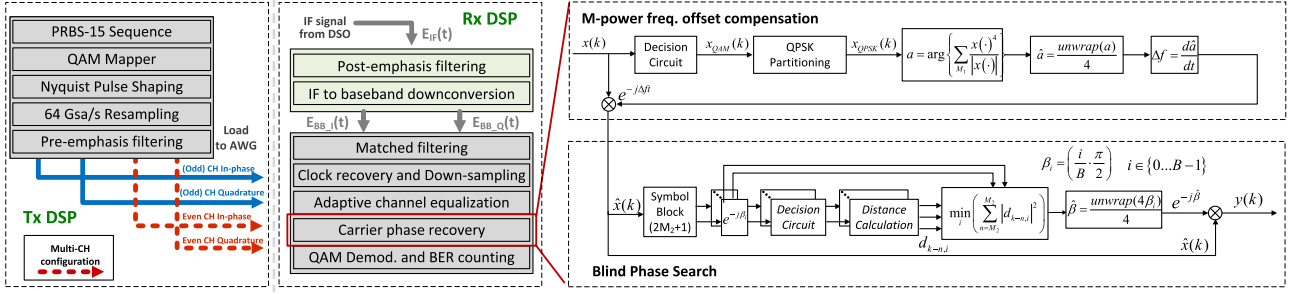


Fig. 4. Block diagrams of the transmitter (Tx) DSP and the receiver (Rx) DSP scheme for the hybrid electro-optical THz transmission systems. The two-stage carrier phase recovery module is elaborated. The first stage is frequency offset compensation based on QPSK partitioning and the M-power method; the second stage is phase noise mitigation based on the blind phase search (BPS) method.

can be transparently frequency-shifted from the optical frequencies to the THz band without distortion. Therefore, one can generate and emit broadband modulated THz signal with such a transmitter scheme.

2) *Detection*: As the THz signals are generally out of the operational range of most broadband receivers, a common practice is to down-convert the signals to an intermediate frequency (IF) band that is detectable by the electronics to perform the further analog-to-digital conversion (ADC) and digital signal processing (DSP). Fig. 3(b) presents the principle of THz signal detection based on coherent frequency down-conversion with a heterodyne receiver, which provides benefits like high spectral efficiency, enhanced receiver sensitivity and SNR compared with envelope extraction based direct detection method [108], [109]. Assuming the incoming THz signal, as expressed in (4), is detected with a Schottky diode and mixed with a local oscillator (LO) signal $E_{LO}(t)$ of amplitude A_{LO} , angular frequency ω_{LO} , and phase φ_{LO} , the down-converted IF signal is then expressed as:

$$\begin{aligned} E_{IF}(t) &= \langle E_{THz}(t) \cdot E_{LO}(t) \rangle \\ &= A_{IF} [I \cdot \sin(\omega_{IF}t + \varphi_{IF}) + Q \cdot \cos(\omega_{IF}t + \varphi_{IF})] \end{aligned} \quad (5)$$

The angle brackets denote low-pass filtering used for rejecting the frequency components at $\omega_{THz} + \omega_{LO}$. $A_{IF} = \eta_{Rx} A_{THz} A_{LO}$, $\omega_{IF} = |\omega_{THz} - \omega_{LO}|$ and $\varphi_{IF} = \varphi_{THz} - \varphi_{LO}$ are the amplitude, the angular frequency, and the phase of the IF signal, respectively. η_{Rx} is the down-conversion efficiency of the mixer. From (5), one can observe that such a coherent heterodyne down-conversion process again preserves the orthogonality of in-phase and quadrature components of the modulated signal, as well as their amplitudes. Up to this point, a THz link supporting broadband signal transmission is established between the THz transmitter and detector. For our transmission experiments, the down-converted IF signal is captured by a real-time digital storage oscilloscope (DSO) and further processed with DSP algorithms compatible with digital coherent optical (DCO) transceivers in fiber-optic systems. It is worth noting that a photonics-assisted THz reception approach was recently demonstrated by directly modulating the incoming THz wave onto an optical carrier with an ultra-broadband plasmonic-organic hybrid (POH) Mach-Zehnder modulator (MZM) of over 360 GHz 3-dB bandwidth [110]. By eliminating the need for

the heterodyne down-converter, such an approach can realize the end-to-end seamless integration with DCO transceivers for fiber-optic systems.

3) *Digital Signal Processing*: Fig. 4 shows the overall DSP routine that we employ for our experimental demonstrations. It consists of the transmitter (Tx) DSP for signal pre-processing before loading to the arbitrary waveform generator (AWG) and the receiver (Rx) DSP for signal post-processing and demodulation. In the Tx DSP, the QAM symbols mapped from the binary data are pulse-shaped with a root-raised-cosine (RRC) filter. An RRC roll-off factor of 0.15 is often used in our experiment. A pre-emphasis filter is used to pre-compensate the AWG's output frequency roll-off. The output signals of the AWG are then used to drive the IQ modulator(s) and create single- or multi-channel optical signals for THz transmissions.

At the receiver, the IF signal captured by the DSO is converted to digital samples for processing. The Rx DSP firstly uses a simple 2-tap post-emphasis filter to compensate for the bandwidth limit of the mixer output. The transfer function of the filter in the Z domain is

$$H(Z) = 1 + \alpha Z^{-1} \quad (6)$$

where α is the post-emphasis coefficient ranging from 0 to -1 . When $\alpha = 0$, there is no post-emphasis, and when $\alpha = -1$, we achieve a maximum post-emphasis with a substantial enhancement of the high-frequency response. A typical value of α is around -0.8 in our sub-THz transmission experiments. Performing such a post-emphasis filtering before rather than after the frequency down-conversion can mitigate the low-pass filtering of the mixer output, which is not symmetrical around the IF carrier but around DC.

After the post-emphasis filter, the digitized real-valued IF signal is further mixed with a digital LO and down-converted to a baseband complex signal expressed as:

$$\begin{aligned} E_{Baseband}(nT_s) &= \langle E_{IF}(nT_s) \cdot e^{-j\omega_{IF}nT_s} \rangle \\ &= \frac{1}{2} j A_{IF} (I + jQ) \cdot e^{j\varphi_{IF}} \end{aligned} \quad (7)$$

where T_s is the sampling period of the digital waveform. The complex-valued baseband digital signal is then processed with the typical DSP routine in digital coherent systems, consisting of matched RRC filtering, clock recovery based on the maximum variance approach, symbol-spaced adaptive equalization based

on lattice filter with the classical butterfly structure driven by the multi-modulus algorithm (MMA) and a 2-stage feedforward carrier phase recovery (CPR) processing. The performance CPR is considered critical for photonics-assisted THz transceivers, where monolithically integrated semiconductor lasers are preferred for carrier generation to reduce the size and footprint. Therefore, we elaborate on the configuration of our 2-stage CPR module in Fig. 4. The first stage is the M-power method-based frequency offset compensation, as the IF down-conversion is often imperfect. Due to the non-uniform distribution of higher-order square QAM signals, the QPSK-partitioning method is adopted to convert the QAM modulation symbols to uniformly distributed QPSK symbols before performing the M-power to remove the modulation [111]. The second stage is based on a modified blind-phase-search (BPS) method [112] with a sliding-window average filter to reduce the influence from additive noise and a quantization noise reduction filter to reduce the required test phase resolution. More detailed studies on the performance of the employed CPR algorithm can be found in [113]. After the CPR, the received QAM symbols are de-mapped into binary data for bit-error-rate (BER) evaluation.

It is noted that some of our experimental studies described in later sections use subcarrier-based OFDM signals, which require a different set of DSP algorithms for channel estimation and phase noise mitigation. Due to the size limit, they are not elaborated on in this paper. Interested readers can refer to [114] for further details.

B. Directly Modulated QCL-Based Free-Space Transmissions in the Upper-THz Band

As we have stated earlier, electromagnetic waves in the upper side of the THz band have closer properties to optics. Therefore, our recent experimental studies focus on free-space transmissions based on directly emitting semiconductor laser sources. More explicitly, we combine a DM QCL with advanced modulation formats and signal processing techniques to explore the system limits. In what follows, we use our experimental configuration as an example and briefly go through the implementation details of the modulation, detection, and DSP techniques.

1) *Modulation and Detection*: The device under test at the free-space transmitter is a distributed feedback (DFB) QCL laser with a center wavelength of $4.65 \mu\text{m}$ ($\sim 64.5 \text{ THz}$) [96]. We mount the QCL chip on a commercial mount (ILX Lightwave LDM-4872) with a Peltier temperature controller (TEC) and a water-cooled base. The QCL is operated at room temperature of 292 K ($19 \text{ }^\circ\text{C}$). The bias current of the QCL is modulated by combining the DC with the modulated signals at a custom-designed bias-tee. The modulated signals in various modulation formats, i.e., NRZ, PAM4, PAM8, and DMT, are pre-processed with transmitter DSP and generated with an AWG. The details of the DSP routines are described in the following subsection. After transmitting over a free-space link, the modulated QCL output is picked up by a commercial MCT (HgCdTe) photovoltaic IR photodetector. Finally, the received signal is converted to digital waveforms for demodulation with receiver DSP routines tailored for each modulation format.

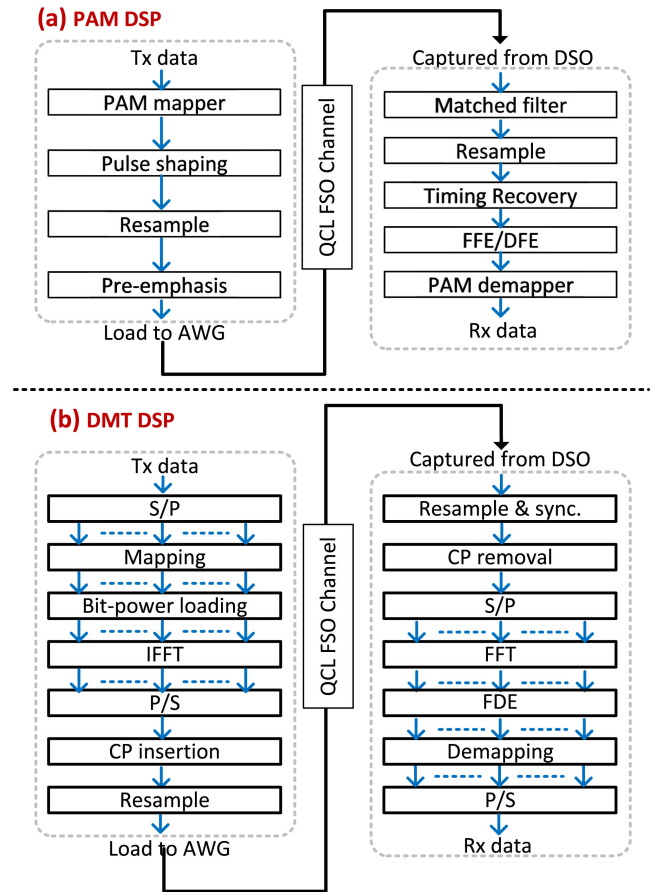


Fig. 5. Block diagrams of the Tx and Rx DSP for (a) PAM. (b) DMT signals for DM QCL-based free-space transmission systems.

2) *Transmitter and Receiver DSP*: Fig. 5 shows the block diagrams of the DSP routines in both the transmitter and the receivers for two types of modulation formats employed, i.e., PAM and DMT. The PAM DSP, as shown in Fig. 5(a), is generically applicable for the two-level NRZ signals and the multilevel PAM4 and PAM8 signals. At the transmitter, the pseudorandom binary data is mapped into PAM symbols and pulse-shaped with an RRC filter. Depending on the targeted signal baud rates, the RRC roll-off factor is usually chosen within the range from 0.01 to 0.2 by optimizing the trade-off between bandwidth and the peak-to-average power ratio (PAPR). Thus, the signal-to-noise ratio (SNR) can be maximized with the same peak-to-peak driving signal amplitude. A static 2-tap pre-emphasis equalizer, which has the same transfer function as (6), is used to pre-compensate the strong low-pass filtering induced by the limited bandwidth of the transceiver. On the receiver side, the captured digital samples firstly pass through a matched RRC filter before being upsampled to 8 samples per symbol. Timing recovery based on maximum variance is performed, and the signal is decimated to 1 sample per symbol for symbol-spaced adaptive equalization. The equalizer is configured either solely as a feed-forward equalizer (FFE) or combined with a decision feedback equalizer (DFE). The equalized symbols are de-mapped into binary bits for BER counting.

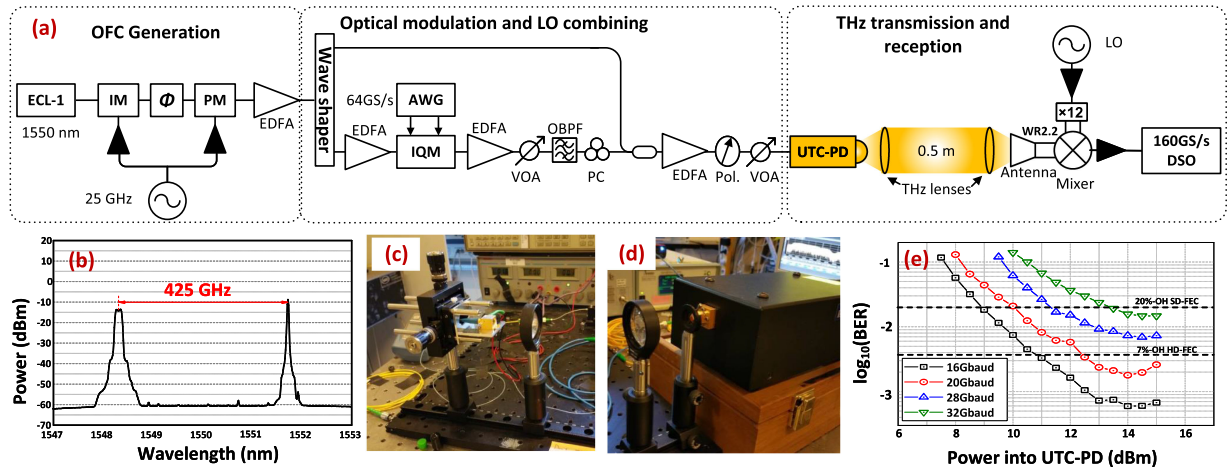


Fig. 6. Single-channel 16QAM signal transmission at 0.4 THz: (a) Experimental setup; (b) the optical spectrum at the UTC-PD; pictures of the (c) THz emitter. (d) THz receiver; and (e) measured BER curves at different baud rates. [53] (IEEE, reprinted with permission).

Fig. 5(b) shows the DSP for generating and demodulating DMT signals. At the transmitter, the serial binary data is first converted to a parallel pattern for the bit-to-symbol mapping. We use Chow's algorithm for the bit- and power-loading to maximize the spectral efficiency of the modulated signal [115]. After the conventional IFFT and parallel-to-serial conversion blocks, we insert the cyclic prefix (CP) and resample the waveform to match the AWG sampling rate. At the receiver, a reverse procedure is performed to recover the parallel symbols modulated on the subcarriers. A simple frequency-domain linear equalizer (FDE) is found to be sufficient for signal equalization in our experiments.

One should note that no complex nonlinear equalizers are used in our experiments. The reason is that both the modulator and the detector have excellent noise performances with a highly linear and large dynamic range for modulation and detection. This is the key factor for transmitting multigigabit data rates over only a few hundred of MHz bandwidth. We further explain and quantify this merit in Section IV.B.

IV. TRANSMISSION SYSTEM EXPERIMENTS

This section presents a few examples of our recent experimental demonstrations of free-space transmissions in both the lower and upper-THz bands, enabled by the methodologies described in Section III.

A. High-Speed Transmissions in the 0.3-0.5 THz Bands With the Hybrid Electro-Optical Approach

1) *Single-Channel THz Transmissions Assisted With Photonics*: Fig. 6 summarizes our experimental study of a single-channel photonic-wireless transmission in the 0.4 THz band. The experimental setup is shown in Fig. 6(a). We firstly use cascaded intensity and phase modulator to generate an optical frequency comb (OFC). Then we use a wave shaper to select the two tones with 425 GHz separation as the two optical carriers for photomixing, as shown in Fig. 6(b). One of the carriers is modulated with single-carrier 16QAM at different baud rates of

up to 32 Gbaud. The two carriers are combined and launched into a broadband UTC-PD for photomixing. The UTC-PD, as shown in Fig. 6(c), is a commercial packaged device integrated with a bow-tie antenna (NTT Electronics Corp, IOD-PMAN-12001). A pair of THz lenses (100-mm diameter, 200-mm focal length) separated with 0.5-meter distance is used to collimate the THz beam. At the receiver, a Schottky Barrier Diode (SBD)-based sub-harmonic mixer (SHM, VDI WR2.2MixAMC) is used to detect the received THz signal. The SHM, as shown in Fig. 6(d), has an IF output bandwidth of 40 GHz and is driven by a 12-time frequency multiplied electrical LO signal. The down-converted IF signal is then captured by the 160 GS/s DSO for offline DSP demodulation.

Fig. 6(e) shows the measured BER curves versus the launched optical power into the UTC-PD. We achieved BER performance below the 7% overhead (OH) hard-decision FEC (HD-FEC) limit of 3.8×10^{-3} with 20 Gbaud 16QAM signal and below the 20% OH soft-decision FEC (SD-FEC) limit of 2×10^{-2} at 32 Gbaud, resulting in a net data rate of 106 Gb/s with stable performance [54].

2) *Multi-Channel Hybrid Electro-Optical THz Transmissions*: We extend our experimental study to a multi-channel configuration and summarize it in Fig. 7 [55]. The experimental setup is shown in Fig. 7(a). A few modifications can be observed compared with our single-channel setup shown in Fig. 6(a). Firstly, we use narrower OFC spacing and use the wave shaper to select six frequency channels, which are grouped in 3 pairs. Secondly, instead of using phase-locked comb lines for heterodyne photomixing, we use a free-running external laser as the optical LO. This is due to the limited spectral coverage of generated frequency comb lines in our experiment. As we described in Section III.A.3), the CPR module can compensate for such a frequency offset and phase noise with a negligible penalty. The optical spectrum of the combined signal and carrier is shown in Fig. 7(b). In this experiment, all six channels are simultaneously emitted by the UTC-PD and transmitted through the free-space link. At the receiver, we adjust the electrical LO frequency and drive the SHM down-converting one channel at a time. The

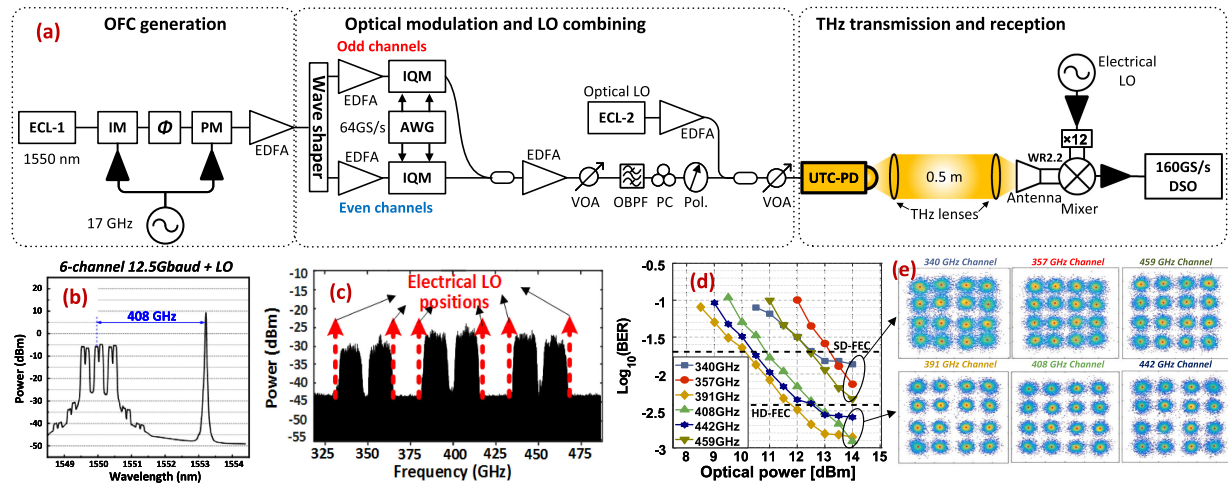


Fig. 7. Multi-channel 16-QAM signal transmission at 0.4 THz: (a) Experimental setup; (b) the optical spectrum at the UTC-PD. (c) Electrical spectra of the THz signals and LO arrangement; (d) measured BER curves for all 6 channels; and (e) the respective signal constellations at optimal power levels. [55] (IEEE, reprinted with permission.).

THz signal spectrum and positions of the electrical LO are illustrated in Fig. 7(c). The channel arrangement and the choice of LO positions are to avoid coherent crosstalk from adjacent channels during the down-conversion. Finally, the measured BER performances for all six channels are shown in Fig 7(d). Due to the different SNR performances among different channels, three of the six channels achieved BER below the HD-FEC limit, whereas the SD-FEC limit was achieved for the other three channels. The selected constellation diagrams for all channels are shown in Fig. 7(e), where clear performance differences among the channels are observed.

To further extend this work towards simultaneous multi-channel reception, one can consider using frequency-division demultiplexers to spatially separate the multiplexed frequency channels [116], [117], or using receiver arrays consisting of multiple coherent detectors with different LO frequencies for active channel selection and filtering. The latter approach resembles the ‘superchannel’ detection scheme in coherent fiber-optic systems and can be facilitated by the recent advancement of large-scale integrated circuits. Both approaches can be potentially applied to detecting multi-channel broadband signals before any fundamental breakthrough in receiver bandwidth occurs.

3) *Extending the Transmission Distance*: Both the single- and multi-channel experimental studies described above were limited in transmission distance. Thus, the next attempt was to increase the link distance. We first lowered the carrier frequency from 0.4 THz to 0.35 THz, gaining higher output power from the UTC-PD. With this configuration, we extended the transmission distance to 2 meters at 100 Gb/s [56]. We further employed a pair of 54 dBi gain Cassegrain reflector antennas, switched to a slightly more energy-efficient PS-16QAM-OFDM modulation format, and demonstrated an indoor transmission over 26.8-m distance at a net rate of 106 Gb/s. The free-space path loss (FSPL) for such a distance for 0.35 THz signal is calculated to be around 112 dB. A picture of the THz transmitter, receiver, and the indoor THz link is shown in Fig. 8(a). The measured BER curve and a selected constellation diagram are shown in Fig. 8(b)

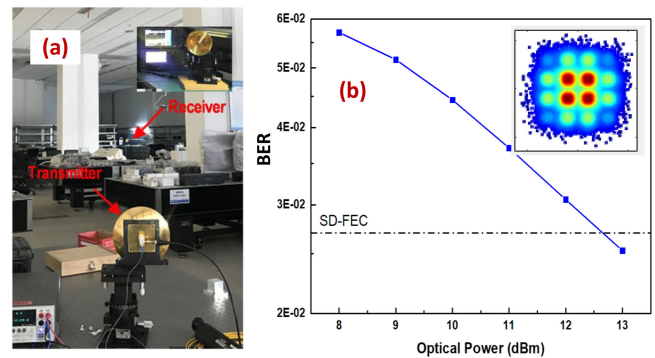


Fig. 8. 106 Gb/s PS-16QAM-OFDM transmission at 0.35 THz over 26.8-m indoor distance: (a) picture of the link configuration in the lab and (b) measured BER curve and a selected constellation diagram. (Reproduced from [59], with the permission of AIP Publishing).

[59]. It is worth noting that no amplifiers at THz frequencies are used in this work. Therefore, further extending the THz wireless distance can be expected with effective THz amplification, as presented in [49].

4) *Multi-Dimensional Multiplexing*: Multiplexing is another key aspect. Indeed, practically, fewer channels may save cost and maximize interface density. From an energy efficiency point of view, it is more reasonable to adopt the concept of ‘parallelism’ than to squeeze more information into a fewer number of channels. Considering total power P_{tot} and number of channels N , the information-theoretic capacity scales linearly in N but only logarithmically in power per channel P_{tot}/N [118]. Therefore, multiplexing has become a trend for research and development in both wireless communications (e.g., MIMO) and fiber-optics (wavelength, polarization, and spatial division multiplexing). Therefore, we consider it is of interest to study the translation of these multiplexing schemes into the sub-THz regime and perform experimental explorations in this aspect. Fig. 9 summarizes the results of our recent experimental study on a joint frequency- and polarization-multiplexed free-space

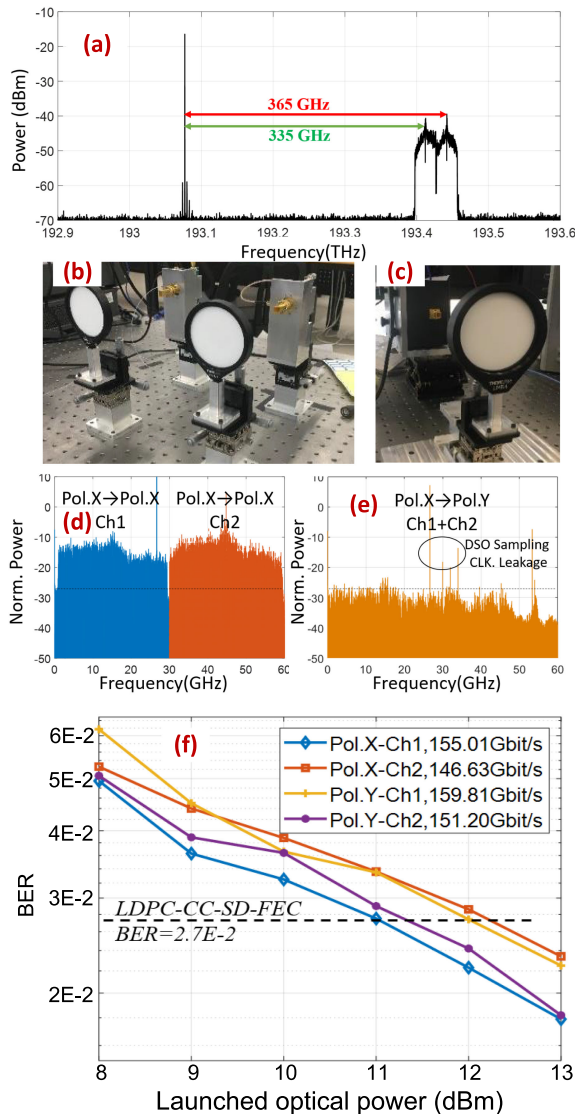


Fig. 9. 2×300 Gb/s PS-64QAM-OFDM transmission at 0.35 THz over 2.8-m free-space link with joint frequency and spatial/polarization multiplexing: (a) the optical spectrum consisting of both the modulated signals and the carrier; the pictures of (b) the two orthogonal polarized THz Tx antennas with collimation lenses and (c) the THz receiver; the combined electrical spectra of the IF signals (d) with aligned polarization states, and (e) with orthogonal states between the Tx and Rx antennas; (f) measured BER curves for all multiplexed channels. [60] (IEEE, reprinted with permission.).

transmission system at 0.35 THz [60]. Two orthogonal polarizations, each carrying two channels multiplexed in the frequency domain, formed four independent channels and were simultaneously emitted and transmitted through the free-space link. The optical spectrum of the two channels of X-polarization captured before the UTC-PD is shown in Fig. 9(a). As a proof-of-concept demonstration, we used a single antenna at the receiver, aligned to one polarization at a time, to detect the transmitted THz signal. The transmitters and the receiver pictures are shown in Fig. 9(b) and (c), respectively. Comparing the electrical spectra shown in Fig. 9(d) and (e), we observed negligible crosstalk from the channels of the orthogonal polarization state. Fig. 9(f) shows the measured BER curves for all four multiplexed channels.

The maximum achievable raw data rates for each channel are shown in the legend. This system's aggregated raw data rate is calculated to be 612.65 Gb/s, resulting in an aggregated net rate of 510.5 Gb/s after extracting the FEC overhead.

B. Multigigabit MWIR Free-Space Transmissions With Directly-Modulated QCL

In this subsection, we summarize our recent experimental works in free-space transmissions in the upper-THz band, enabled by a directly-modulated QCL emitting at $4.65 \mu\text{m}$.

1) *4 Gb/s Close-Proximity Transmission With DMT and PAM4*: Fig. 10 summarizes our first experimental trials of the QCL-based MWIR free-space transmission. The experimental setup is shown in Fig. 10(a). The pictures of the QCL mount and the MCT detector are shown in the insets. The QCL chip was manufactured by mirSense, and the MCT IR PD was a commercial unit (Vigo System SA). Due to the mechanical mismatches, in this study, we didn't install the collimating lens on the QCL mount, and the QCL chip and the MCT detector were only separated with a 5-cm distance. The P-I-V curve of the QCL is shown in Fig. 10(b). A maximum continuous optical power of 60 mW can be achieved at 350 mA driving current. Two modulation formats, i.e., PAM4 and DMT, were tested with this setup. The signals of the two modulation formats were generated and detected with the DSP routines described in Sec. III. B. The measured S21 frequency response of the end-to-end link is shown in Fig. 10(c). The 3-dB bandwidth is only around 320 MHz, and the 6-dB bandwidth is around 440 MHz. The bottleneck of the system bandwidth is believed to be the MCT PD, which has a 3-dB bandwidth of 720 MHz per the manufacturer's specifications. For PAM4 modulation at 2 Gbaud, we used a pronounced pre-emphasis filtering with coefficient $\alpha = -0.99$ to enhance the high-frequency components. The signal spectra before and after the free-space transmission are also shown in Fig. 10(c). One can see that the received signal spectrum is equalized to a regular QAM signal spectral shape owing to the pre-emphasis filtering. The BER curves and the selected eye diagram are shown in Fig. 10(d) and (e), respectively. With a 13-tap FFE, we could achieve performance below the HD-FEC limit. Clear eye openings are also observed. For DMT, we tested configurations both with and without bit- and power-loading. Fig. 10(f) shows the corresponding bit-loading mapping. The BER performance of the DMT transmissions is summarized in Fig. 10(g). The maximum achievable data rate benchmarked against the HD-FEC limit was explored for different configurations, and the one with bit- and power-loading gave the highest achievable rate.

Finally, considering the pulse shaping and the strong pre-emphasis for PAM4 and the bit- and power-loading configuration for DMT both result in high PAPR values, such a transmission performance verified the excellent noise performances and the high linearity of this system.

2) *0.5-m Collimated Beam Transmission With PAM Signals*: Considering the limited link distance in the first round of our experiment, we performed a follow-up experiment with a re-design of the custom bias-tee, which enabled the installation

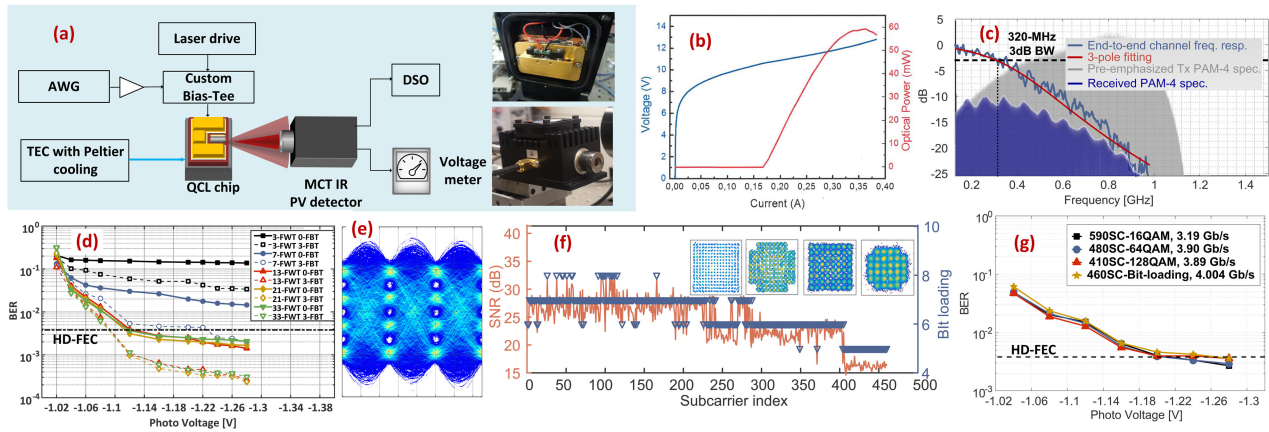


Fig. 10. (a) Experimental setup of 4 Gb/s free-space transmission with the 4.65- μm DM QCL. (b) P-I-V curve of the QCL. (c) End-to-end S21 response and equalized signal spectrum before and after transmission. (d) BER performance of 2 Gbaud PAM4. (e) Eye diagram of the equalized 2 Gbaud PAM4 signal. (f) SNR and bit-loading configuration of 4 Gb/s DMT signal. (g) BER performance of DMT signals at various bit rates. [104].

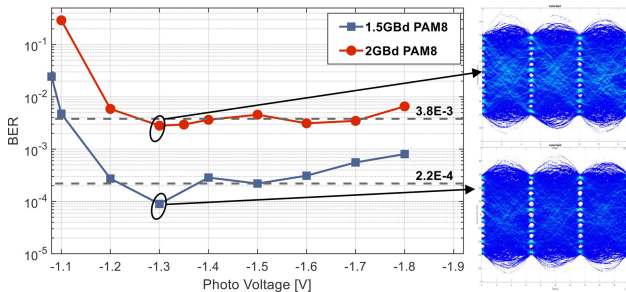
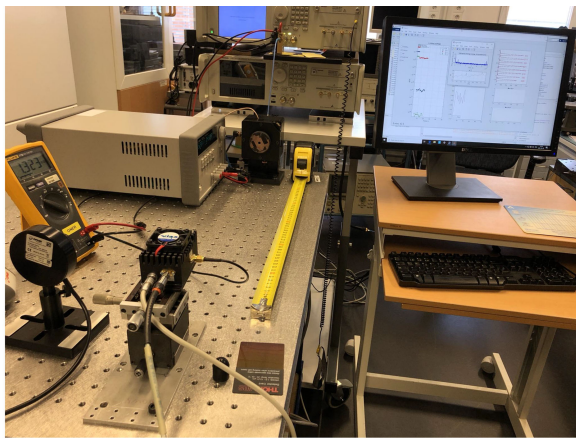


Fig. 11. Up to 6 Gb/s PAM8 free-space transmission with the 4.65- μm DM QCL over extended reach of 0.5 meter. [105].

of a collimating lens on the QCL mount. With proper beam collimation, we could considerably increase the transmission distance and enhance the received SNR [105], [106]. Fig. 11 shows a picture of the tabletop experimental setup and the transmission results of PAM8 signals. In this experiment, we set a 0.5-m link distance between the QCL output and the MCT PD due to the space constraints of the setup. 1.5 Gbaud PAM8 signal, corresponding to a bit rate of 4.5 Gb/s, was transmitted through the link, and received with a BER performance below the KP4-FEC limit of $2.2\text{E-}4$ [119]. Furthermore, 2 Gbaud PAM8, corresponding to a bit rate of 6 Gb/s, was achievable against

the HD-FEC threshold. Finally, we could confidently expect a much longer transmission distance from the measured BER curves, considering the large power margin shown in the current system.

V. CONCLUSION

We present an overview of the current research and development status for free-space communications in the underexploited THz spectrum region, consisting of both the lower-THz band, i.e., the sub-MMW, and the upper-THz band, i.e., the MWIR and LWIR. Photonic technologies have started to show irreplaceable merits in many of these high-speed transmission systems at high carrier frequencies. One can expect them to play an increasingly important role in the envisioned technological roadmap shift towards an all-spectra communication paradigm. Our experimental contributions in both the lower- and upper-THz bands are summarized. In the lower-THz region, we adopt the hybrid electro-optical approach based on heterodyne photomixing and transparently translate broadband modulation from the fiber-optic wavelength to the THz frequency. In the upper-THz region, we adopt a DM QCL as the signal source and experimentally demonstrate multigigabit transmission at room temperature. Following the path towards future development, technical challenges exist in both THz regions. In the lower-THz region, the limited THz output power and the low-conversion efficiency of the electro-optical approach hinder the development of energy-efficient transceiver solutions. Possible ways forward are to employ transmitter arrays to increase emitting power and perform large-scale co-integration of photonics and electronics to reduce power loss. In the upper-THz band, further increasing the supportable data rate with the QCL-based approach is the near-term target. It requires engineering effort on the transmitter side to reduce the parasitic effect during fabrication and packaging and more fundamental effort on the detector side to achieve high bandwidth at room temperature. Recent progress in developing ultrafast MWIR/LWIR photodetectors, including both the quantum well infrared photodetectors (QWIPs) and the quantum cascade detectors (QCDs), has shown promising

results in supporting over 50 GHz detection bandwidth at room temperature [120]–[123]. Combining these novel components and devices with advanced multiplexing techniques, one can expect orders of magnitude higher transmission data rates supportable in the MWIR/LWIR bands. For both the lower- and upper-THz regions, to establish complete free-space communication system solutions supporting necessary functionalities such as multi-dimensional multiplexing and beamforming, research and development of all relevant active and passive components and devices will be necessary, including external modulators, amplifiers, filters, wavelength/spatial selective switches and so on. Finally, identifying a viable approach to bridge further the gap between the lower- and upper-THz regions is essential to exploit the rich spectral resource in the THz band and achieve the all-spectra communication target. One of the high potential candidates is the THz-QCL, considering its recent breakthroughs in demonstrations of high-speed modulation [124] and room-temperature operation [125]. Considering all these aspects, further research efforts in this underexploited direction can be highly rewarding.

ACKNOWLEDGMENT

The authors would like to thank Francesco Da Ros, Pengyu Guan, Michael Galili and Darko Zibar from DTU SPOC, Shiwei Wang and Hongqi Zhang from Zhejiang University, and Prof. Gunnar Jacobsen from RISE for offering their insights during the studies of the lower-THz transmission systems. Gregory Maisons and Mathieu Carras from mirSense are acknowledged for providing us with the QCL chip.

REFERENCES

- [1] T. S. Rappaport *et al.*, “Millimeter wave mobile communications for 5G cellular: It will work!,” *IEEE Access*, vol. 1, pp. 335–349, 2013.
- [2] Ericsson mobility report Q2 update, Aug. 2021. [Online]. Available: <https://www.ericsson.com/4a4cd9/assets/local/reports-papers/mobility-report/documents/2021/emr-q2-2021-update.pdf>
- [3] W. Shi, J. Cao, Q. Zhang, Y. Li, and L. Xu, “Edge computing: Vision and challenges,” *IEEE Internet Things J.*, vol. 3, no. 5, pp. 637–646, Oct. 2016.
- [4] E. Björnson, E. G. Larsson, and T. L. Marzetta, “Massive MIMO: Ten myths and one critical question,” *IEEE Commun. Mag.*, vol. 54, no. 2, pp. 114–123, Feb. 2016.
- [5] X. You *et al.*, “Towards 6G wireless communication networks: Vision, enabling technologies, and new paradigm shifts,” *Sci. China Inf. Sci.*, vol. 64, no. 1, pp. 110301:1–110301:74, 2020.
- [6] A. Delga, L. Leviandier, M. Razeghi, J. S. Lewis, G. A. Khodaparast, and E. Tournié, “Free-space optical communications with quantum cascade lasers,” in *Proc. Quantum Sens. Nano Electron. Photon. XVI*, 2019, vol. 10926, pp. 1092617.
- [7] X. Pang *et al.*, “Free-Space transmissions in the upper- and lower-THz bands assisted with photonics,” in *Proc. Eur. Conf. Opt. Commun.*, Bordeaux, France, 2021, pp. 1–4.
- [8] A. Hirata *et al.*, “120-GHz-Band Wireless link technologies for outdoor 10-Gbit/s data transmission,” *IEEE Trans Microw. Theory Tech.*, vol. 60, no. 3, pp. 881–895, Mar. 2012.
- [9] H. Takahashi, T. Kosugi, A. Hirata, J. Takeuchi, K. Murata, and N. Kukutsu, “120-GHz-band fully integrated wireless link using QSPK for realtime 10-Gbit/s transmission,” *IEEE Trans Microw. Theory Tech.*, vol. 61, no. 12, pp. 4745–4753, Dec. 2013.
- [10] H. Song *et al.*, “Demonstration of 20-Gbps wireless data transmission at 300 GHz for KIOSK instant data downloading applications with InP MMICs,” in *Proc. IEEE MTT-S Int. Microw. Symp.*, San Francisco, CA, USA, 2016, pp. 1–4.
- [11] F. Boes *et al.*, “Ultra-broadband MMIC-based wireless link at 240 GHz enabled by 64GS/s DAC,” in *Proc. 39th Int. Conf. Infrared, Millimeter, Terahertz waves*, 2014, pp. 1–2.
- [12] I. Kallfass *et al.*, “64 Gbit/s transmission over 850 m fixed wireless link at 240 GHz carrier frequency,” *J. Infrared, Millimeter, Terahertz Waves*, vol. 36, no. 2, pp. 221–233, 2015.
- [13] I. Kallfass *et al.*, “Towards MMIC-based 300 GHz indoor wireless communication systems,” *IEICE Trans. Electron.*, vol. E98.C, no. 12, pp. 1081–1090, 2015.
- [14] H. Hamada *et al.*, “300-GHz. 100-Gb/s InP-HEMT wireless transceiver using a 300-GHz fundamental mixer,” in *Proc. IEEE/MTT-S Int. Microw. Symp.*, Philadelphia, PA, USA, 2018, pp. 1480–1483.
- [15] Z. Niu *et al.*, “The research on 220 GHz multicarrier high-speed communication system,” *China Commun.*, vol. 17, no. 3, pp. 131–139, 2020.
- [16] I. Dan, G. Ducournau, S. Hisatake, P. Szriftgiser, R.-P. Braun, and I. Kallfass, “A terahertz wireless communication link using a superheterodyne approach,” *IEEE Trans. Terahertz Sci. Technol.*, vol. 10, no. 1, pp. 32–43, Jan. 2020.
- [17] K. Katayama *et al.*, “A 300 GHz CMOS transmitter with 32-QAM 17.5 Gb/s/ch capability over six channels,” *IEEE J. Solid-State Circuits*, vol. 51, no. 12, pp. 3037–3048, Dec. 2016.
- [18] K. Takano *et al.*, “17.9 A 105 Gb/s 300 GHz CMOS transmitter,” in *Proc. IEEE Int. Solid-State Circuits Conf.*, San Francisco, CA, USA, 2017, pp. 308–309.
- [19] S. Lee *et al.*, “An 80-Gb/s 300-GHz-band single-chip CMOS transceiver,” *IEEE J. Solid-State Circuits*, vol. 54, no. 12, pp. 3577–3588, Dec. 2019.
- [20] P. Rodríguez-Vázquez, J. Grzyb, B. Heinemann, and U. R. Pfeiffer, “A 16-QAM 100-Gb/s 1-M wireless link with an EVM of 17% at 230 GHz in a sige technology,” *IEEE Microw. Wireless Compon. Lett.*, vol. 29, no. 4, pp. 297–299, Apr. 2019.
- [21] P. Rodriguez-Vazquez, J. Grzyb, B. Heinemann, and U. R. Pfeiffer, “A QPSK 110-Gb/s polarization-diversity MIMO wireless link with a 220–255 GHz tunable LO in a sige HBT technology,” *IEEE Trans Microw. Theory Tech.*, vol. 68, no. 9, pp. 3834–3851, Sep. 2020.
- [22] Y. Nishida, N. Nishigami, S. Diebold, J. Kim, M. Fujita, and T. Nagatsuma, “Terahertz coherent receiver using a single resonant tunnelling diode,” *Sci. Rep.s*, vol. 9, no. 1, 2019.
- [23] J. Webber, N. Nishigami, J. Y. Kim, M. Fujita, and T. Nagatsuma, “Terahertz wireless communications using resonant tunnelling diodes with radio-over-fibre,” *Electron. Lett.*, vol. 55, no. 17, pp. 949–951, 2019.
- [24] S. Iwamatsu, N. Nishigami, Y. Nishida, M. Fujita, and T. Nagatsuma, “Resonant tunneling diode array oscillator integrated with slot-ring antenna for terahertz wireless communications,” in *Proc. 45th Int. Conf. Infrared, Millimeter, Terahertz Waves*, 2020, pp. 1–2.
- [25] A. J. Seeds, “Microwave photonics,” *IEEE Trans Microw. Theory Tech.*, vol. 50, no. 3, pp. 877–887, Mar. 2002.
- [26] A. J. Seeds and K. J. Williams, “Microwave photonics,” *J. Lightw. Technol.*, vol. 24, no. 12, pp. 4628–4641, 2006.
- [27] J. Capmany and D. Novak, “Microwave photonics combines two worlds,” *Nature Photon.*, vol. 1, no. 6, pp. 319–330, Jun. 2007.
- [28] J. Yao, “Microwave photonics,” *J. Lightw. Technol.*, vol. 27, no. 3, pp. 314–335, 2009.
- [29] T. Nagatsuma, G. Ducournau, and C. C. Renaud, “Advances in terahertz communications accelerated by photonics,” *Nature Photon.*, vol. 10, no. 6, pp. 371–379, 2016.
- [30] A. Kanno *et al.*, “20-Gb/s QPSK W-band (75–110GHz) wireless link in free space using radio-over-fiber technique,” *IEICE Electron. Exp.*, vol. 8, no. 8, pp. 612–617, 2011.
- [31] A. Kanno *et al.*, “40 Gb/s W-band (75–110 GHz) 16-QAM radio-over-fiber signal generation and its wireless transmission,” *Opt. Exp.*, vol. 19, no. 26, pp. B56–B63, 2011.
- [32] X. Pang *et al.*, “100 Gbit/s hybrid optical fiber-wireless link in the W-band (75–110 GHz),” *Opt. Exp.*, vol. 19, no. 25, pp. 24944–24949, Dec. 2011.
- [33] X. Pang *et al.*, “25 Gbit/s QPSK hybrid fiber-wireless transmission in the W-Band (75–110 GHz) with remote antenna unit for in-building wireless networks,” *IEEE Photon. J.*, vol. 4, no. 3, pp. 691–698, Jun. 2012.
- [34] Y. Yoshimizu, S. Hisatake, S. Kuwano, J. Terada, N. Yoshimoto, and T. Nagatsuma, “Wireless transmission using coherent terahertz wave with phase stabilization,” *IEICE Electron. Exp.*, vol. 10, no. 18, 2013, Art. no. 20130578.
- [35] X. Pang, A. Lebedev, J. J. Vegas Olmos, and I. Tafur Monroy, “Multigigabit W-band (75–110 GHz) bidirectional hybrid fiber-wireless systems in access networks,” *J. Lightw. Technol.*, vol. 32, no. 23, pp. 3983–3990, 2014.

- [36] J. Zhang, J. Yu, N. Chi, Z. Dong, X. Li, and G.-K. Chang, "Multi-channel 120-Gb/s data transmission over 2×2 MIMO fiber-wireless link at W-Band," *IEEE Photon. Technol. Lett.*, vol. 25, no. 8, pp. 780–783, Apr. 2013.
- [37] X. Li, J. Yu, J. Zhang, Z. Dong, F. Li, and N. Chi, "A 400 G optical wireless integration delivery system," *Opt Exp.*, vol. 21, no. 16, pp. 18812–18819, 2013.
- [38] X. Li *et al.*, "1-Tb/s millimeter-wave signal wireless delivery at D-band," *J. Lightw. Technol.*, vol. 37, no. 1, pp. 196–204, 2019.
- [39] Y. Uemura, Y. Kawamoto, N. Shibata, L. Yi, and T. Nagatsuma, "600-GHz-band heterodyne receiver system using photonic techniques," in *Proc. Int. Topical Meeting Microw. Photon.*, 2020, pp. 256–259.
- [40] T. Ishibashi, N. Shimizu, S. Kodama, H. Ito, T. Nagatsuma, and T. Furuta, "Uni-traveling-carrier photodiodes," *Ultrafast Electron. Optoelectron.*, vol. 13, p. UC3, 1997.
- [41] T. Ishibashi and H. Ito, "Uni-traveling-carrier photodiodes," *J. Appl. Phys.*, vol. 127, no. 3, 2020, Art. no. 031101.
- [42] H. Shams *et al.*, "100 Gb/s multicarrier THz wireless transmission system with high frequency stability based on a gain-switched laser comb source," *IEEE Photon. J.*, vol. 7, no. 3, Jun. 2015, Art. no. 7902011.
- [43] S. Koenig *et al.*, "Wireless sub-THz communication system with high data rate," *Nature Photon.*, vol. 7, no. 12, pp. 977–981, 2013.
- [44] V. K. Chinni *et al.*, "Single-channel 100 Gbit/s transmission using III–V UTC-PDs for future IEEE 802.15.3d wireless links in the 300 GHz band," *Electron. Lett.*, vol. 54, no. 10, pp. 638–640, 2018.
- [45] T. Harter *et al.*, "Wireless THz link with optoelectronic transmitter and receiver," *Optica*, vol. 6, no. 8, pp. 1063–1070, 2019.
- [46] X. Li *et al.*, "132-Gb/s photonics-aided single-carrier wireless terahertz-wave signal transmission at 450 GHz enabled by 64QAM modulation and probabilistic shaping," in *Proc. Opt. Fiber Commun. Conf.*, San Diego, CA, USA, 2019, pp. 1–3.
- [47] C. Castro *et al.*, "32 Gbd 16QAM wireless transmission in the 300 GHz band using a PIN diode for THz upconversion," in *Opt. Fiber Commun. Conf.*, San Diego, CA, USA, 2019, pp. 1–3.
- [48] I. Dan *et al.*, "A 300-GHz wireless link employing a photonic transmitter and an active electronic receiver with a transmission bandwidth of 54 GHz," *IEEE Trans. Terahertz Sci. Technol.*, vol. 10, no. 3, pp. 271–281, May 2020.
- [49] T. Harter *et al.*, "Generalized Kramers–Kronig receiver for coherent terahertz communications," *Nature Photon.*, vol. 14, no. 10, pp. 601–606, 2020.
- [50] X. Yu *et al.*, "400-GHz wireless transmission of 60-Gb/s Nyquist-QPSK signals using UTC-PD and heterodyne mixer," *IEEE Trans. Terahertz Sci. Technol.*, vol. 6, no. 6, pp. 765–770, Nov. 2016.
- [51] X. Yu *et al.*, "160 Gbit/s photonics wireless transmission in the 300–500 GHz band," *APL Photon.*, vol. 1, no. 8, 2016, Art. no. 081301.
- [52] S. Jia *et al.*, "120 Gb/s multi-channel THz wireless transmission and THz receiver performance analysis," *IEEE Photon. Technol. Lett.*, vol. 29, no. 3, pp. 310–313, Feb. 2017.
- [53] X. Pang *et al.*, "Single channel 106 Gbit/s 16QAM wireless transmission in the 0.4 THz band," in *Proc. Opt. Fiber Commun.*, Los Angeles, CA, USA, 2017, pp. 1–3.
- [54] S. Jia *et al.*, "0.4 THz photonic-wireless link with 106 Gb/s single channel bitrate," *J. Lightw. Technol.*, vol. 36, no. 2, pp. 610–616, 2018.
- [55] X. Pang *et al.*, "260 Gbit/s photonic-wireless link in the THz band," in *Proc. IEEE Photon. Conf.*, Waikoloa, HI, USA, 2016, pp. 1–2.
- [56] K. Liu *et al.*, "100 Gbit/s THz photonic wireless transmission in the 350-GHz band with extended reach," *IEEE Photon. Technol. Lett.*, vol. 30, no. 11, pp. 1064–1067, Jun. 2018.
- [57] S. Jia *et al.*, "Integrated dual-DFB laser for 408 GHz carrier generation enabling 131 Gbit/s wireless transmission over 10.7 meters," in *Proc. Opt. Fiber Commun. Conf.*, San Diego, CA, 2019, pp. 1–3.
- [58] A. Udalcovs *et al.*, "107.1-Gbps net-rate transmission over a joint 51km-fibre-and-10.7m-wireless link for terahertz radio access networks," in *Proc. Eur. Conf. Opt. Commun.*, 2019, pp. 1–4.
- [59] S. Wang *et al.*, "26.8-m THz wireless transmission of probabilistic shaping 16-QAM-OFDM signals," *APL Photon.*, vol. 5, no. 5, 2020, Art. no. 056105.
- [60] S. Jia *et al.*, " 2×300 Gbit/s line rate PS-64QAM-OFDM THz photonic-wireless transmission," *J. Lightw. Technol.*, vol. 38, no. 17, pp. 4715–4721, Sep. 2020.
- [61] H. Zhang *et al.*, "Tbit/s multi-dimensional multiplexing THz-over-fiber for 6G wireless communication," *J. Lightw. Technol.*, vol. 39, no. 18, pp. 5783–5790, 2021.
- [62] C. Castro, R. Elschner, T. Merkle, C. Schubert, and R. Freund, "Experimental demonstrations of high-capacity THz-wireless transmission systems for beyond 5G," *IEEE Commun. Mag.*, vol. 58, no. 11, pp. 41–47, Nov. 2020.
- [63] T. Nagatsuma, "THz communication systems," in *Proc. Opt. Fiber Commun. Conf. Exhibit*, 2017, pp. Tu3B.1.
- [64] H.-J. Song, K. Ajito, Y. Muramoto, A. Wakatsuki, T. Nagatsuma, and N. Kukutsu, "24 Gbit/s data transmission in 300 GHz band for future terahertz communications," *Electron. Lett.*, vol. 48, no. 15, pp. 953–954, 2012.
- [65] T. Nagatsuma *et al.*, "Real-time 100-Gbit/s QPSK transmission using photonics-based 300-GHz-band wireless link," in *Proc. IEEE Int. Topical Meeting Microw. Photon.*, Long Beach, CA, USA, 2016, pp. 27–30.
- [66] J. Webber, A. Oshiro, S. Iwamatsu, Y. Nishida, M. Fujita, and T. Nagatsuma, "48-Gbit/s 8K video-transmission using resonant tunnelling diodes in 300-GHz band," *Electron. Lett.*, vol. 57, no. 17, pp. 668–669, 2021.
- [67] T. Nagatsuma, T. Kurokawa, M. Sonoda, T. Ishibashi, M. Shimizu, and K. Kato, "600-GHz-band waveguide-output uni-traveling-carrier photodiodes and their applications to wireless communication," in *Proc. IEEE/MTT-S Int. Microw. Symp. - IMS*, Philadelphia, PA, USA, 2018, pp. 1180–1183.
- [68] T. Nagatsuma, M. Sonoda, T. Higashimoto, L. Yi, and J. Hesler, "vol. 12.5-Gbit/s wireless link at 720 GHz based on photonics," in *Proc. 44th Int. Conf. Infrared, Millimeter, Terahertz Waves*, 2019, pp. 1–2.
- [69] Y. Uemura, Y. Kawamoto, N. Shibata, L. Yi, and T. Nagatsuma, "600-GHz-band heterodyne receiver system using photonic techniques," in *Proc. Int. Topical Meeting Microw. Photon.*, 2020, pp. 256–259.
- [70] I. F. Akyildiz, C. Han, Z. Hu, S. Nie, and J. M. Jornet, "TeraHertz band communication: An old problem revisited and research directions for the next decade," 2021, doi: [10.48550/arXiv.2112.13187](https://doi.org/10.48550/arXiv.2112.13187).
- [71] A. V. Okishev and J. D. Zuegel, "Intracavity-pumped Raman laser action in a mid-IR, continuous-wave (cw) MgO:PPLN optical parametric oscillator," *Opt. Exp.*, vol. 14, no. 25, pp. 12169–12173, 2006.
- [72] E. Ip *et al.*, "QPSK transmission over free-space link at 3.8 μm using coherent detection with wavelength conversion," in *Proc. 34th Eur. Conf. Opt. Commun.*, 2008, pp. 1–2.
- [73] K.-D. F. Büchter, H. Herrmann, C. Langrock, M. M. Fejer, and W. Sohler, "All-optical Ti:PPLN wavelength conversion modules for free-space optical transmission links in the mid-infrared," *Opt. Lett.*, vol. 34, no. 4, pp. 470–472, Feb. 2009.
- [74] P. Cho *et al.*, "Optical homodyne RZ-QPSK transmission through wind tunnel at 3.8 and 1.55 micron via wavelength conversion," *SPIE Defense, Secur., Sens.*, vol. 7324, 2009, Art. no. 73240A.
- [75] Q. Hao *et al.*, "Mid-infrared transmitter and receiver modules for free-space optical communication," *Appl. Opt.*, vol. 56, no. 8, pp. 2260–2264, 2017.
- [76] Y. Su *et al.*, "10 Gbps DPSK transmission over free-space link in the mid-infrared," *Opt. Exp.*, vol. 26, no. 26, pp. 34515–34528, 2018.
- [77] W. Wang *et al.*, "5 Gbaud QPSK coherent transmission in the mid-infrared," *Opt. Commun.*, vol. 466, 2020, Art. no. 125681.
- [78] K. Zou *et al.*, "Demonstration of free-space 300-Gbit/s QPSK communications using both wavelength- and mode- division-multiplexing in the mid-IR," in *Proc. Opt. Fiber Commun.*, San Francisco, CA, USA, 2021, pp. 1–3.
- [79] R. Dentí, P. A. Andrekson, H. Ahlberg, and S. T. Eng, "3.5 μm optical communication experiment at 100 mbits–1 using a PbCdS diode laser," *Opt. Quantum Electron.*, vol. 21, no. 1, pp. 69–72, 1989.
- [80] J. Faist, F. Capasso, D. L. Sivco, C. Sirtori, A. L. Hutchinson, and A. Y. Cho, "Quantum cascade laser," *Science*, vol. 264, no. 5158, pp. 553–556, 1994.
- [81] J. Faist *et al.*, "Distributed feedback quantum cascade lasers," *Appl. Phys. Lett.*, vol. 70, no. 20, pp. 2670–2672, 1997.
- [82] M. Beck *et al.*, "Continuous wave operation of a mid-infrared semiconductor laser at room temperature," *Science*, vol. 295, no. 5553, pp. 301–305, 2002.
- [83] N. Mustafa, L. Pesquera, C. Y. L. Cheung, and K. A. Shore, "Terahertz bandwidth prediction for amplitude modulation response of unipolar intersubband semiconductor lasers," *IEEE Photon. Technol. Lett.*, vol. 11, no. 5, pp. 527–529, May 1999.
- [84] R. Martini *et al.*, "High-speed modulation and free-space optical audio/video transmission using quantum cascade lasers," *Electron. Lett.*, vol. 37, no. 3, pp. 191–193, 2001.

- [85] R. Martini *et al.*, "High-speed digital data transmission using mid-infrared quantum cascade lasers," *Electron. Lett.*, vol. 37, no. 21, pp. 1290–1292, 2001.
- [86] F. Capasso *et al.*, "Quantum cascade lasers: Ultrahigh-speed operation, optical wireless communication, narrow linewidth, and far-infrared emission," *IEEE J. Quantum Electron.*, vol. 38, no. 6, pp. 511–532, Jun. 2002.
- [87] R. Martini *et al.*, "Free-space optical transmission of multimedia satellite data streams using mid-infrared quantum cascade lasers," *Electron. Lett.*, vol. 38, no. 4, pp. 181–183, 2002.
- [88] S. Blaser, D. Hofstetter, M. Beck, and J. Faist, "Free-space optical data link using Peltier-cooled quantum cascade laser," *Electron. Lett.*, vol. 37, no. 12, pp. 778–780, 2001.
- [89] M. Taslakov, S. Mecherle, V. Simeonov, and H. van den Bergh, "Line-of-sight data transmission system based on Mid IR quantum cascade laser," in *Proc. Free-Space Laser Commun. Technol. XX*, vol. 6877, 2008, Art. no. 68770F.
- [90] A. Soibel *et al.*, "Midinfrared interband cascade laser for free space optical communication," *IEEE Photon. Technol. Lett.*, vol. 22, no. 2, pp. 121–123, Jan. 2010.
- [91] B. S. Williams, "Terahertz quantum-cascade lasers," *Nature Photon.*, vol. 1, no. 9, pp. 517–525, Sep. 2007.
- [92] Z. Chen *et al.*, "Wireless communication demonstration at 4.1 THz using quantum cascade laser and quantum well photodetector," *Electron. Lett.*, vol. 47, no. 17, pp. 1002–1003, 2011.
- [93] Z. T. Zhiyong Tan, Z. C. Zhen Chen, J. C. Juncheng Cao, and H. L. Huichun Liu, "Wireless terahertz light transmission based on digitally-modulated terahertz quantum-cascade laser," *Chin. Opt. Lett.*, vol. 11, no. 3, pp. 031403–031405, 2013.
- [94] Z. Chen, L. Gu, Z. Tan, C. Wang, and J. C. Cao, "Real-time video signal transmission over a terahertz communication link," *Chin. Opt. Lett.*, vol. 11, no. 11, pp. 112001–112003, 2013.
- [95] L. Gu, Z. Tan, Q. Wu, C. Wang, and J. Cao, "20 Mbps wireless communication demonstration using terahertz quantum devices," *Chin. Opt. Lett.*, vol. 13, no. 8, pp. 081402–081404, 2015.
- [96] M. Carras *et al.*, "Room-temperature continuous-wave metal grating distributed feedback quantum cascade lasers," *Appl. Phys. Lett.*, vol. 96, no. 16, 2010, Art. no. 161105.
- [97] Y. H. Zhou *et al.*, "High-speed quantum cascade laser at room temperature," *Electron. Lett.*, vol. 52, no. 7, pp. 548–549, 2016.
- [98] C. Liu *et al.*, "Free-space communication based on quantum cascade laser," *J. Semiconductors*, vol. 36, no. 9, 2015, Art. no. 094009.
- [99] E. Luzhansky, F.-S. Choa, S. Merritt, A. Yu, and M. Krainak, "Mid-IR free-space optical communication with quantum cascade lasers," in *Laser Radar Technol. Appl. XX; Atmospheric Propag. XII*, 2015, Art. no. 946512.
- [100] J. J. Liu *et al.*, "Mid and long-wave infrared free-space optical communication," in *Proc. Laser Commun. Propag. Through Atmos. Oceans VIII*, 2019, Art. no. 1113302.
- [101] O. Spitz *et al.*, "Free-space communication with directly modulated mid-infrared quantum cascade devices," *IEEE J. Sel. Topics Quantum Electron.*, vol. 28, no. 1, pp. 1–9, Jan./Feb. 2022.
- [102] X. Pang *et al.*, "Gigabit free-space multilevel signal transmission with a mid-infrared quantum cascade laser operating at room temperature," *Opt. Lett.*, vol. 42, no. 18, pp. 3646–3649, 2017.
- [103] X. Pang *et al.*, "4 Gbps PAM-4 and DMT free space transmission using a 4.65- μm quantum cascaded laser at room temperature," in *Proc. Eur. Conf. Opt. Commun.*, Gothenburg, Sweden, 2017, pp. 1–3.
- [104] X. Pang *et al.*, "Free-space communications enabled by quantum cascade lasers," *Physica Status Solidi (a)*, vol. 218, no. 3, 2021, Art. no. 2000407.
- [105] X. Pang *et al.*, "Up to 6 Gbps mid-infrared free-space transmission with a directly modulated quantum cascade laser," in *Proc. Eur. Conf. Opt. Commun.*, Bordeaux, France, 2021, pp. 1–4.
- [106] X. Pang *et al.*, "Direct modulation and Free-space transmissions of up to 6 Gbps multilevel signals with a 4.65- μm quantum cascade laser at room temperature," *J. Lightw. Technol.*, early access, 2021, doi: [10.1109/JLT.2021.3137963](https://doi.org/10.1109/JLT.2021.3137963).
- [107] H. Dely *et al.*, "10 Gbit s^{-1} free space data transmission at 9 μm wavelength with unipolar quantum optoelectronics," *Laser Photon. Rev.*, vol. 16, no. 2, 2022, Art. no. 2100414.
- [108] M. Qiao *et al.*, "60 Gbit/s PAM-4 wireless transmission in the 310 GHz band with nonlinearity tolerant signal processing," *Opt. Commun.*, vol. 492, 2021, Art. no. 126988.
- [109] L. Zhang *et al.*, "Nonlinearity-aware optoelectronic terahertz discrete multitone signal transmission with a zero-bias diode," *Opt. Lett.*, vol. 45, no. 18, pp. 5045–5048, 2020.
- [110] S. Ummethala *et al.*, "THz-to-optical conversion in wireless communications using an ultra-broadband plasmonic modulator," *Nature Photon.*, vol. 13, no. 8, pp. 519–524, 2019.
- [111] I. Fatadin, D. Ives, and S. J. Savory, "Laser linewidth tolerance for 16-QAM coherent optical systems using QPSK partitioning," *IEEE Photon. Technol. Lett.*, vol. 22, no. 9, pp. 631–633, May 2010.
- [112] T. Pfau, S. Hoffmann, and R. Noe, "Hardware-efficient coherent digital receiver concept with feedforward carrier recovery for M-QAM constellations," *J. Lightw. Technol.*, vol. 27, no. 8, pp. 989–999, 2009.
- [113] J. R. Navarro *et al.*, "High performance and low complexity carrier phase recovery schemes for 64-QAM coherent optical systems," in *Proc. Opt. Fiber Commun. Conf. Exhibit*, Los Angeles, CA, USA, 2017, pp. 1–3.
- [114] W. Shieh, H. Bao, and Y. Tang, "Coherent optical OFDM: Theory and design," *Opt. Exp.*, vol. 16, no. 2, pp. 841–859, Jan. 2008.
- [115] P. Chow, J. M. Cioffi, and J. A. C. Bingham, "A practical discrete multi-tone transceiver loading algorithm for data transmission over spectrally shaped channels," *IEEE Trans. Commun.*, vol. 43, nos. 2/3/4, pp. 773–775, Feb.-Apr. 1995.
- [116] N. J. Karl, R. W. McKinney, Y. Monnai, R. Mendis, and D. M. Mittleman, "Frequency-division multiplexing in the terahertz range using a leaky-wave antenna," *Nature Photon.*, vol. 9, no. 11, pp. 717–720, 2015.
- [117] J. Ma, N. J. Karl, S. Bretin, G. Ducournau, and D. M. Mittleman, "Frequency-division multiplexer and demultiplexer for terahertz wireless links," *Nature Commun.*, vol. 8, no. 1, pp. 1–8, 2017.
- [118] J. M. Kahn and D. A. B. Miller, "Communications expands its space," *Nature Photon.*, vol. 11, no. 1, pp. 5–8, 2017.
- [119] *IEEE standard for ethernet amendment 2: physical layer specifications and management parameters for 100 Gb/s operation over backplanes and copper cables*, in IEEE Std 802.3bj-2014 (Amendment to IEEE Std 802.3-2012 as amended by IEEE Std 802.3bk-2013), pp. 1–368, Sep. 2014, doi: [10.1109/IEEESTD.2014.6891095](https://doi.org/10.1109/IEEESTD.2014.6891095).
- [120] D. Palaferri *et al.*, "Room-temperature nine- μm -wavelength photodetectors and GHz-frequency heterodyne receivers," *Nature*, vol. 556, no. 7699, pp. 85–88, 2018.
- [121] M. Hakl *et al.*, "Ultrafast quantum-well photodetectors operating at 10 μm with a flat frequency response up to 70 GHz at room temperature," *ACS Photon.*, vol. 8, no. 2, pp. 464–471, 2021.
- [122] J. Hillbrand *et al.*, "High-speed quantum cascade detector characterized with a mid-infrared femtosecond oscillator," *Opt. Exp.*, vol. 29, no. 4, pp. 5774–5781, 2021.
- [123] A. Delga, "8 - Quantum cascade detectors: A review," in *Mid-infrared Optoelectronics*, E. Tournié and L. Cerutti Eds.: Woodhead Publishing, 2020, pp. 337–377.
- [124] A. Dunn *et al.*, "High-speed modulation of a terahertz quantum cascade laser by coherent acoustic phonon pulses," *Nature Commun.*, vol. 11, no. 1, 2020, Art. no. 835.
- [125] A. Khalatpour, A. K. Paulsen, C. Deimert, Z. R. Wasilewski, and Q. Hu, "High-power portable terahertz laser systems," *Nature Photon.*, vol. 15, no. 1, pp. 16–20, 2021.